ADVANCED MATERIALS INTERFACES
www.advmatinterfaces.de

Thickness Dependence of Interface-Generated Spin Currents in Ferromagnet/Ti/CoFeB Trilayers

Gaeun Choi, Jeongchun Ryu, Sungjun Lee, Jaimin Kang, Namgyu Noh, Jong Min Yuk, and Byong-Guk Park**

Interface-generated spin currents in ferromagnet (FM)/nonmagnet (NM) structures provide both in-plane and out-of-plane spin–orbit torques (SOTs), enabling the field-free switching of perpendicular magnetization of the other FM layer in magnetic trilayers. In this study, the NM thickness dependence of interface-generated spin currents and associated SOTs in FM/Ti/CoFeB trilayers is investigated. In such magnetic trilayers, it is known that the in-plane SOT results from the spin–orbit filtering of the interface-generated spin current, while the out-of-plane SOT is due to the spin–orbit precession. These results show that the polarity of current-induced magnetization switching under an in-plane magnetic field reverses with increasing Ti thickness. This indicates that the sign of the in-plane SOT depends on the current distribution between the bottom FM and Ti layers. On the other hand, field-free switching occurs only for a Ti thickness of up to ≈4 nm, and the same polarity is retained, demonstrating that out-of-plane SOT is governed by the charge current flowing near the interface. These results suggest that field-free switching efficiency can be enhanced by engineering the relative conductance of the FM/NM bilayers to constructively combine in-plane and out-of-plane SOTs caused by interface-generated spin currents.

1. Introduction

Electrical generation of a spin current via spin–orbit coupling (SOC) has been a central topic in spintronic research since spin current efficiently controls the magnetization direction of ferromagnet (FM).[1–11] The spin Hall effect (SHE) and Rashba–Edelstein effect are typical examples and have been widely investigated in recent years. The former creates a transverse spin current in a nonmagnet (NM) with strong SOC. When an electric field **E** is applied in the *x*-direction, a spin current flowing along the *z*-direction carries a spin polarization in the *y*-direction.[12–21] The latter generates a spin density at the NM/FM interfaces with inversion asymmetry.[22–30] Both mechanisms induce spin accumulations, which exert spin torques and manipulate the magnetization direction of the FM layer.

Recent studies have revealed another spin current generation mechanism. In the so-called interface-generated spin current,[31–35] the FM/NM interface gives rise to sizable spin currents. A charge current flowing into the FM/NM bilayer creates nonequilibrium carriers with a momentum perpendicular to the interface due to different electrical conductivities between the FM and NM layers. These carriers subsequently undergo interface scattering due to the spin–orbit field, $\mathbf{B}_{so}$, formed at the FM/NM interface. Note that the direction of $\mathbf{B}_{so}$ ($//y$) is orthogonal to both **E** ($//x$) and the direction normal to the film plane ($//z$). There are two interfacial spin scattering mechanisms due to $\mathbf{B}_{so}$: spin–orbit filtering (SOF) and spin–orbit precession (SOP). SOF applies to the parallel component of the spins to $\mathbf{B}_{so}$, with parallel (antiparallel) spins preferentially transmitted (reflected) at the interface (**Figure 1**a). Thus, the SOF-induced spin current carries a spin polarization along $\mathbf{B}_{so}$ ($//y$) identical to the spin Hall or Rashba–Edelstein-induced spin currents. However, the SOP occurs when the transverse components of the spins interact with $\mathbf{B}_{so}$ at the interface. Because the spin polarization of the charge carriers in FM is aligned to its magnetization direction **m**, the spin polarization of the SOP-induced spin current is in the $\mathbf{m} \times \mathbf{B}_{so}$ direction (Figure 1b). In this mechanism, when **m** is in the *x*-direction, the SOP generates a spin current with out-of-plane ($//z$) spin polarization. This allows field-free SOT switching of the perpendicular magnetization, which is one of the most important technological issues in SOT-based spintronic devices.[3,7,9,11,31,34–45] Note that field-free SOT switching by out-of-plane spin current has also been demonstrated in various systems including an FM/ferroelectric structure,[46] a tilted magnetic anisotropy,[47,48] a structural asymmetry.[49,50] However, the critical current density of the SOT switching is still too large for device applications; therefore, it is very important to develop a way to reduce the switching current density while being capable of field-free

G. Choi, J. Ryu,[+] S. Lee, J. Kang, N. Noh, J. M. Yuk, B.-G. Park
Department of Materials Science and Engineering
KAIST
Daejeon 34141, Korea
E-mail: jc.ryu@samsung.com; bgpark@kaist.ac.kr

The ORCID identification number(s) for the author(s) of this article can be found under https://doi.org/10.1002/admi.202201317.

[+]Present address: Samsung Advanced Institute of Technology, Suwon 16678, Korea

DOI: 10.1002/admi.202201317

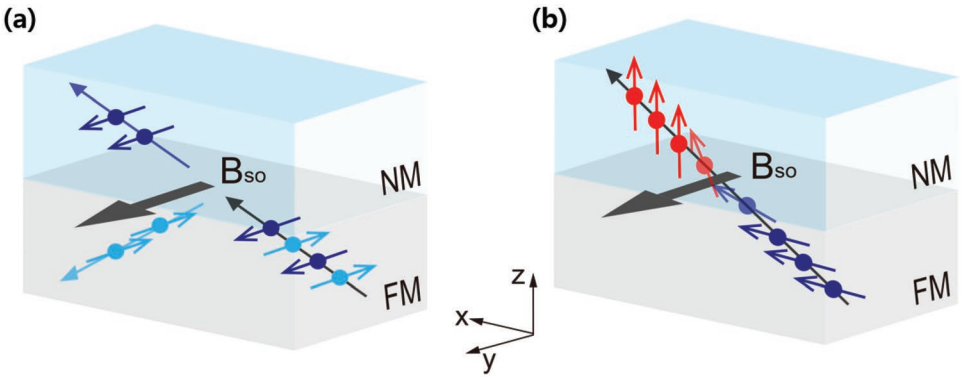

Figure 1. Mechanisms of interface-generated spin currents. a) Spin–orbit filtering (SOF): a spin current parallel (antiparallel) to spin–orbit field ($\mathbf{B}_{so}$) is transmitted (reflected) at the interface. The transmitted (reflected) spins are described in dark blue (light blue) arrows. b) Spin–orbit precession (SOP): a transverse spin current to $\mathbf{B}_{so}$ undergoes precession at the interface, resulting in a spin polarization of $\mathbf{m} \times \mathbf{B}_{so}$ direction, where $\mathbf{m}$ is the magnetization direction of FM. When $\mathbf{m}$ is aligned to the *x*-direction, a spin current with out-of-plane spin polarization is generated.

switching. In the magnetic trilayers, where the SOF and SOP of the interface-generated spin current create in-plane and out-of-plane SOTs, respectively, it is reasonable to assume that field-free switching efficiency can be improved by the constructive combination of the spin currents generated by SOF and SOP. To this end, systematic material investigation is required for a deeper understanding of the interface-generated spin current.

In this work, we investigate interface-generated spin currents and associated switching behaviors in FM/Ti/CoFeB trilayer structures as a function of Ti thickness. We first examine in-plane SOT by measuring current-induced magnetization switching in the presence of an in-plane magnetic field. The magnetization switching polarity is reversed as the Ti thickness increases, and the critical Ti thickness at which the switching polarity changes depends on the electrical conductivity of the bottom FM. This demonstrates that the in-plane SOT in the trilayer, primarily induced by SOF-induced spin currents, is determined by the relative current distribution between the bottom FM and Ti layers. On the other hand, the field-free magnetization switching shows different behaviors; the field-free switching is successful only for a Ti thickness of up to 4 nm and its polarity remains the same regardless of the Ti thickness. This indicates that the out-of-plane SOT due to the SOP spin current responsible for field-free switching is independent of the charge current distribution. However, the smaller flow of current near the interface with increasing Ti thickness suggests that out-of-plane SOT originates from the FM/Ti interface. Our findings show that by controlling the conductivities, it is possible to manipulate the interface-generated spin currents, allowing the in-plane and out-of-plane SOTs to be combined in such a manner that field-free switching is facilitated with a reduced critical current.

2. Results and Discussion

2.1. Sample Characterization in Magnetic Trilayers

We fabricated trilayer samples of FM (4 nm)/Ti (t_{Ti} nm)/CoFeB (1 nm)/MgO (3.2 nm)/Ta (2 nm) structures by magnetron sputtering, with a Ti thickness t_{Ti} of 1–6 nm (**Figure 2**a). Figure 2b shows the high-angle annular dark-field scanning transmission electron microscopy (HAADF-STEM) images of the samples, confirming the quality of the sample, with each layer forming a uniform film. Note that elemental maps of the structures obtained from energy dispersive spectrometry are provided in Section S1 (Supporting Information). We use two different bottom FMs: one CoFeB and the other NiFe. The samples are, hereafter, referred to as the CoFeB-sample and the NiFe-sample, according to the bottom FM. The magnetic properties of the trilayer samples were examined by a vibrating sample magnetometer. The in-plane hysteresis loops of the CoFeB-sample and NiFe-sample shown in Figure 2b and Figure 2c, respectively, demonstrate the in-plane magnetic anisotropy of the bottom FM in the *x*-direction developed by the magnetic field during deposition. Moreover, perpendicular magnetic anisotropy is exhibited in the top CoFeB layer of both samples, as indicated by the out-of-plane hysteresis loops (Figure 2d).

2.2. Current-Induced Magnetization Switching in FM/Ti/CoFeB Trilayers

To examine the interface-generated spin currents and associated SOTs in the FM/Ti/CoFeB trilayer, we perform current-induced magnetization switching measurement with and without an external magnetic field B_x along the current direction.[14–16,51–58] It is noted that both in-plane and out-of-plane SOTs caused by the SOF and SOP spin currents, respectively, always contribute to the current-induced magnetization switching regardless of the application of B_x. However, in the presence of B_x, in-plane SOT dominates the current-induced magnetization switching since the magnitude of in-plane SOT is larger than that of out-of-plane SOT in the magnetic trilayers.[35] In contrast, in the absence of B_x, in-plane SOT cannot switch the magnetization direction alone without out-of-plane SOT, so we can evaluate out-of-plane SOT by measuring field-free SOT switching. Note that the top Ti/CoFeB interface can also generate spin current; however, its contribution to the interface-generated spin currents is negligibly small.[31]

For switching measurements, a current pulse I_p of a 15 μs width was injected, and the anomalous Hall resistance R_H was

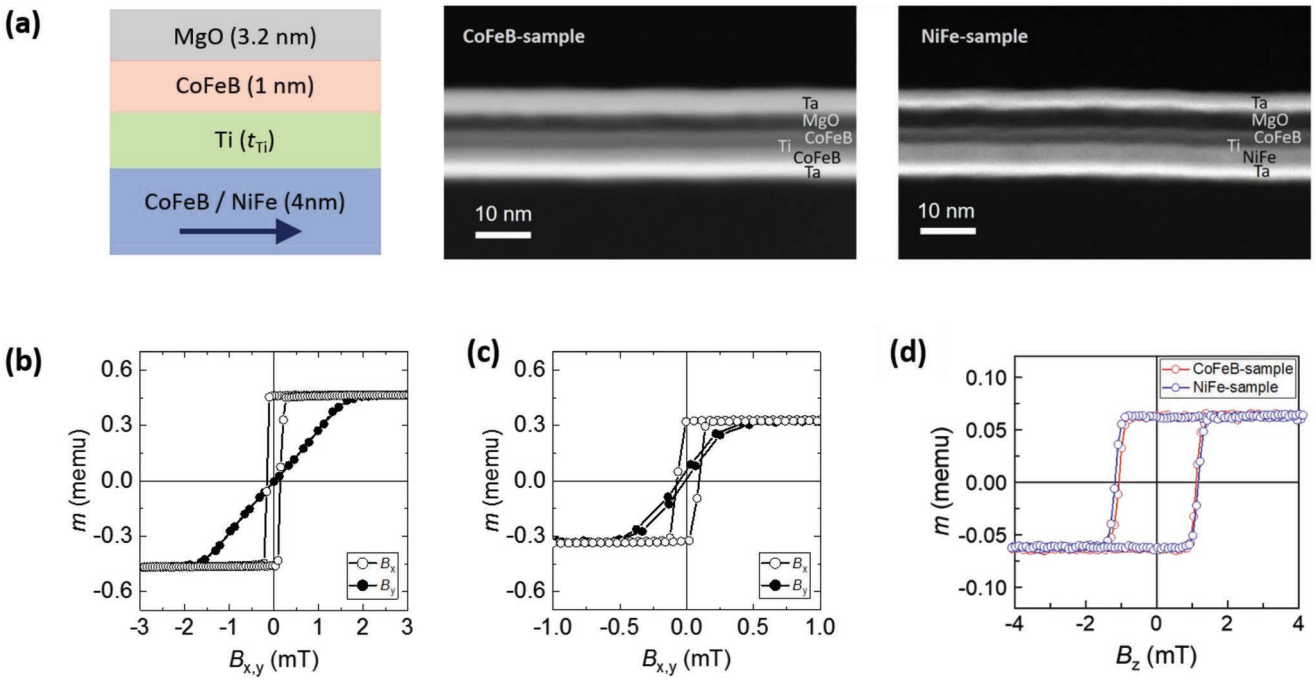

Figure 2. a) Material stack and HAADF-STEM images of a trilayer structure of CoFeB-sample and NiFe-sample, where Ti thickness t_{Ti} varies from 1 to 6 nm. b,c) In-plane hysteresis loops of b) the CoFeB-samples and c) NiFe-samples. Here, the open (filled) circles represent the results measured with a magnetic field $B_{x\,(y)}$ along the *x*- (*y*-)direction. d) Out-of-plane hysteresis loops of the top CoFeB in the CoFeB-samples (red circles) and NiFe-samples (blue circles). The full out-of-plane hysteresis loops of the samples are shown in Section S2 (Supporting Information).

then read to detect the magnetization state. We first present the t_{Ti}-dependent switching behaviors of the CoFeB-samples. **Figure 3**a shows the current-induced magnetization switching under a B_x of 30 mT; the switching polarity is counter clockwise in the case of the CoFeB-sample with t_{Ti} = 1 nm, with a positive current favoring the magnetization switching of the up-to-down direction. Interestingly, magnetization switching is not observed when t_{Ti} = 2 nm, and switching polarity becomes clockwise when t_{Ti} is larger than 3 nm. This indicates that the direction of the in-plane SOT reverses with increasing t_{Ti}. Magnetization switching without B_x is shown in Figure 3b. Field-free switching is obtained for a t_{Ti} of up

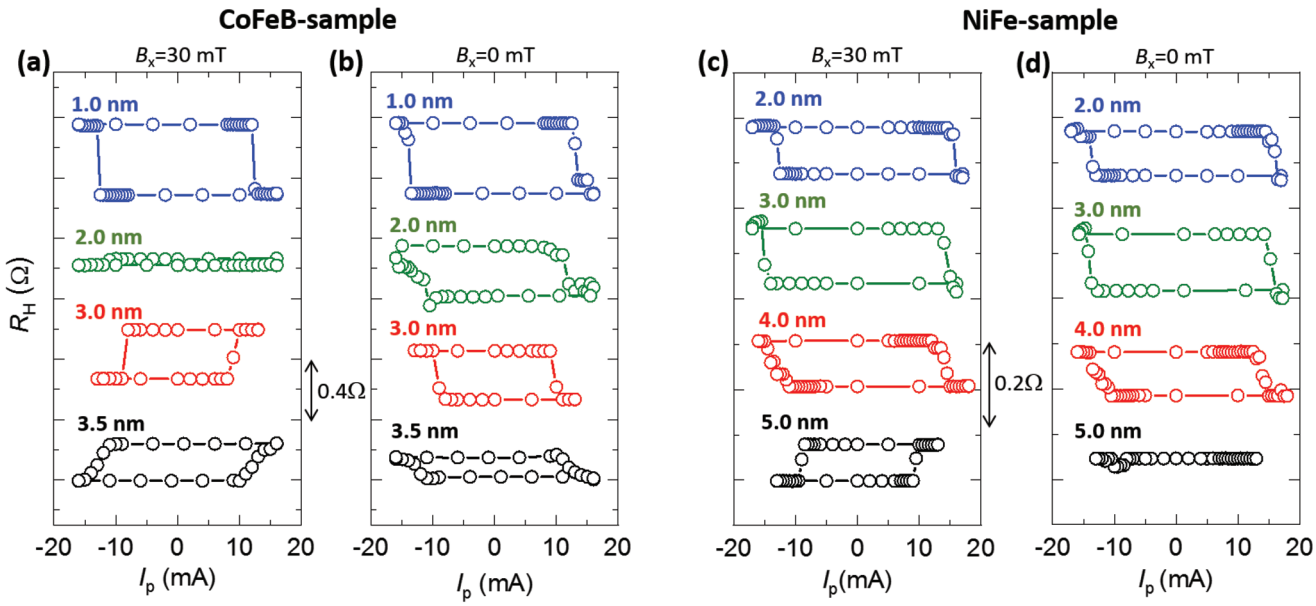

Figure 3. Current-induced magnetization switching as a function of t_{Ti} in a,b) the CoFeB-samples and c,d) the NiFe-samples. The measurements were done a,c) with a B_x of 30 mT and b,d) without B_x.

to 3.5 nm, with the switching polarity remaining constant. Note that it is not possible to investigate CoFeB-samples with a t_{Ti} thickness of >3.5 nm since the perpendicular magnetic anisotropy of the top CoFeB is only obtained at the t_{Ti} below 3.5 nm.

The switching measurements of the NiFe-samples in Figure 3c,d show a similar trend of t_{Ti} dependence to that of the CoFeB-samples. In the case of the NiFe-samples, the switching polarity under a B_x of 30 mT is reversed with increasing t_{Ti}, and field-free switching exhibits the same polarity for a t_{Ti} up to 4 nm. Note that field-free SOT switching has been reported in a similar trilayer structure,[36] where interlayer coupling induces an in-plane magnetic field breaking the switching symmetry. However, the magnitude of interlayer coupling in our sample is found to be too small to significantly affect the current-induced SOT switching (Section S3, Supporting Information).

Note that the critical Ti thickness at which the switching polarity is reversed is larger for the NiFe-sample (4–5 nm) than for the CoFeB-sample (≈2 nm). This result may explain the reason for the opposite effective spin Hall angle between the NiFe/Ti and CoFeB/Ti bilayers when t_{Ti} is equally 3.0 nm in the previous report.[31] The sign reversal of the SOT switching with a B_x suggests that the in-plane SOT governed by the SOF spin currents is related to the relative current distribution between the Ti and FM layers, which depends on the thickness and electrical conductivity of the bottom FM. It is found that the switching current is minimized at t_{Ti} = 3 nm (5 nm) for the CoFeB (NiFe)-sample. This may result from the constructive combination of in-plane and out-of-plane SOTs, as will be discussed in latter sections. On the other hand, the critical current of the field-free switching shows different behaviors. First, there is no sign change with t_{Ti}; therefore, it can be concluded that the SOP spin currents generating out-of-plane SOT is independent of the charge current distribution. Second, field-free switching is absent in the samples with a larger t_{Ti}, indicating that the SOP spin currents and associated out-of-plane SOT are reduced with less charge current flowing near the interface (Section S4, Supporting Information). It is also observed that no field-free switching occurs in samples with a larger bottom FM thickness (Section S5, Supporting Information). Note that there seems to be a particular t_{Ti}, where the field-free switching current is minimized; in the case of the CoFeB-sample, it is t_{Ti} = 3 nm. This suggests that field-free switching efficiency can be improved by the constructive combination of in-plane and out-of-plane SOTs.

Note that in-plane and out-of-plane spin currents can be generated by the bulk FM layer. The former is due to the spin Hall effect in the FM layer[59–61] while the latter is due to the magnetic spin Hall effect,[62–64] spin swapping effect,[65,66] or spin rotation symmetry.[33] Because of the identical symmetry between the magnetization direction of the bottom FM, an applied electric field, and the spin polarization of the generated spin current, it is very difficult to experimentally distinguish the interface-generated spin current (SOF or SOP) from those bulk effects. However, it was reported that the SOT in similar magnetic trilayer structures mainly originates from the FM/Ti interfaces in our previous work.[31]

2.3. Harmonic Hall Voltage Measurement in FM/Ti/CoFeB Trilayers

To quantitatively investigate the in-plane SOT in the trilayers, we perform harmonic Hall voltage measurements.[17,67–70] **Figure 4** shows the representative results of the first and second harmonic Hall resistances $R_{1\omega}$ and $R_{2\omega}$ as a function of B_x, which is associated with the damping-like SOT responsible for magnetization switching. As can be seen by the $R_{1\omega}$ versus B_x curves of the CoFeB-sample and NiFe-sample in Figure 4a and Figure 4b, respectively, the magnetization gradually rotates from out-of-plane to in-plane directions as B_x increases. On the other hand, the $R_{2\omega}$ strongly depends on t_{Ti}. In the case of the CoFeB-samples, the $R_{2\omega}$ of the sample with t_{Ti} = 1.0 nm is positive at a positive B_x and becomes negative when t_{Ti} = 3.0 nm (Figure 4c). The same sign reversal of $R_{2\omega}$ with increasing t_{Ti} is seen in the NiFe-sample (Figure 4d). Figure 4e,f shows the obtained effective magnetic field B_{DL} induced by the damping-like SOT using $B_{DL} = -2(dR_{2\omega}/dB_x)/(dR_{1\omega}^2/dB_x^2)$ as a function of t_{Ti} for a current density of 1×10^7 A cm^{-2}. As was found in the switching experiments (see Figure 3a,c), B_{DL} gradually decreases and changes its sign with increasing t_{Ti}. Note that there is a slight difference in the t_{Ti} at the point where the sign inversion for the harmonic Hall measurement occurs. This can likely be attributed to the contribution to magnetization switching made by the out-of-plane SOT, which is expected even in the presence of B_x. Note that the current-induced Oersted field and field-like SOT can contribute to the in-plane SOT. However, their magnitude is much smaller than that of the damping-like SOT; therefore, it is assumed that their contribution to the current-induced magnetization switching is not significant (Section S3, Supporting Information).

2.4. Relative Charge Current Distribution and Interface-Generated Spin Currents

To investigate the correlation between the SOF spin currents (and associated in-plane SOT) and the current distribution in the bottom FM and Ti layers, we estimate the ratio of charge currents flowing through the FM and Ti layers. **Figure 5**a shows the resistance R of Ti, CoFeB, and NiFe in CoFeB-sample and NiFe-sample as a function of t_{Ti}. The extracted resistivities ρ of the FM and Ti layers are ρ_{CoFeB} = 189 μΩ cm, ρ_{NiFe} = 81 μΩ cm, and ρ_{Ti} = 182 μΩ cm. Using the parallel circuit model,[71–74] we calculate the relative charge current flowing through the Ti (FM) layer $I_{Ti(FM)}/I_0$, where I_0 is the total current. As can be seen in Figure 5b, I_{Ti}/I_0 becomes larger than I_{FM}/I_0 when t_{Ti} is greater than 4 nm (9 nm) for the CoFeB-sample (NiFe-sample). The sign change of the SOF spin currents (J_S) flowing in the $+z$ direction can be explained in terms of the charge current distribution. That is, the J_S is predominantly governed by the spin transmission at the FM/Ti interface in the sample with a thin Ti (Figure 5c), where a large portion of the charge currents flows to the bottom FM layer ($I_{c,\,Ti} < I_{c,\,FM}$). Therefore, spin polarization is carried parallel to $\mathbf{B}_{so}$. On the other hand, in samples with a large Ti thickness ($I_{c,\,Ti} > I_{c,\,FM}$, Figure 5d), the J_S is dominated by the spin

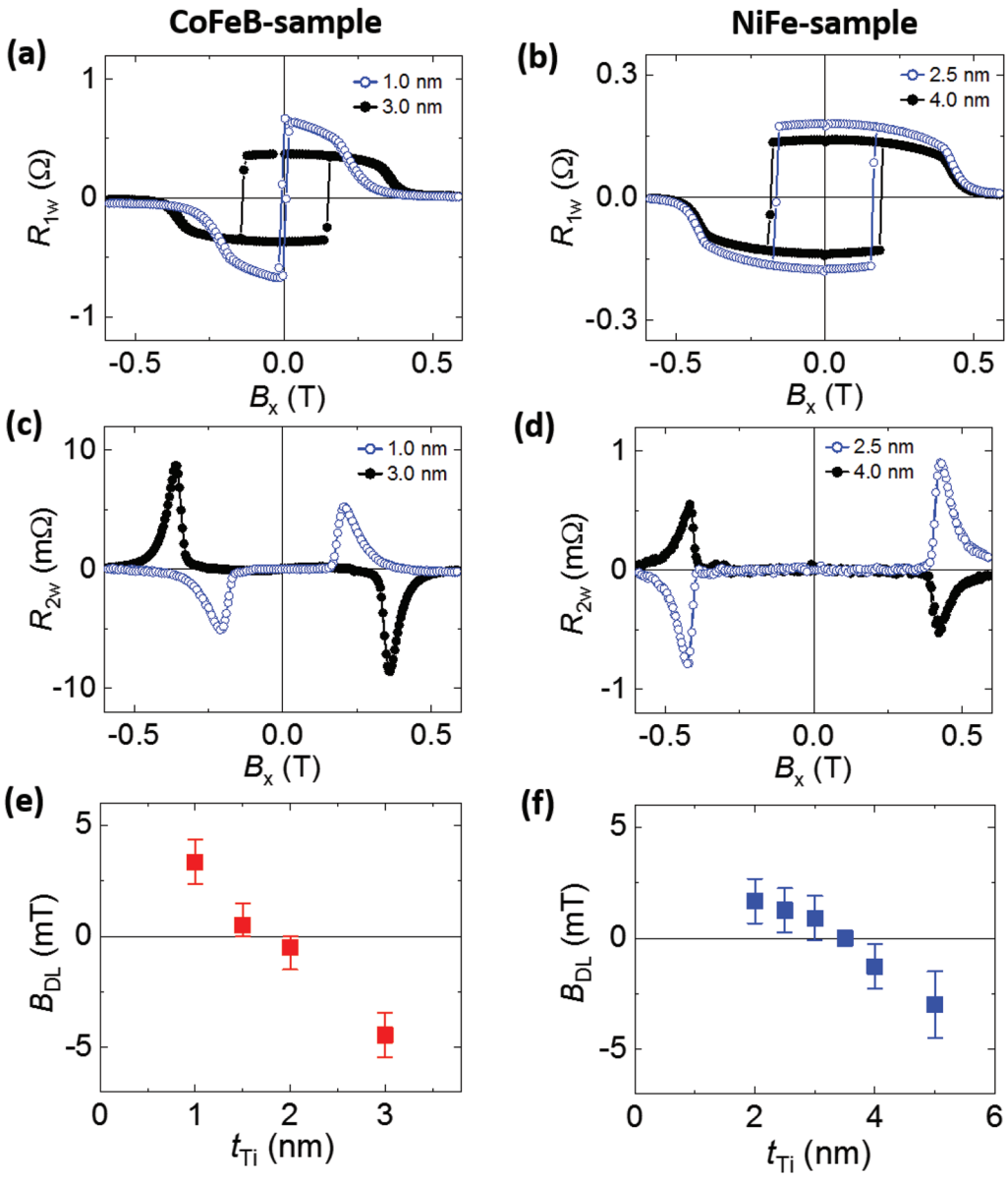

Figure 4. Harmonic Hall voltage measurements as a function of t_{Ti}. a–d) The representative results of the first and second harmonic Hall resistances a,b) $R_{1\omega}$ and c,d) $R_{2\omega}$ measured with a B_x in the a,c) CoFeB-samples and b,d) NiFe-samples. e,f) Damping-like SOT (B_{DL}) for a current density of 1×10^7 A cm^{-2} as a function of t_{Ti} in the e) CoFeB-samples and f) NiFe-samples.

reflection at the FM/Ti interface, resulting in spin polarization antiparallel to $\mathbf{B}_{so}$. Consequently, the sign of the in-plane SOT caused by SOF spin currents is determined by the current distribution in the FM/Ti bilayers. Note that that it is likely that the absence of a sign change in the field-free switching polarity means that the SOP spin current is independent of the charge current distribution. However, due to the limitations of this study, this was not confirmed experimentally and remains a matter for further investigation.

3. Conclusion

In this work, we investigate the interface-generated spin currents in the FM/Ti/CoFeB trilayer structure as a function of the t_{Ti} using current-induced switching and harmonic Hall voltage measurements. It is found that the in-plane SOT changes its sign with increasing t_{Ti}. This indicates that the SOF spin current is determined by spin transmission/reflection at the FM/Ti interface depending on the current distribution between the bottom FM and the Ti layer. Furthermore, we find that the out-of-plane SOT responsible for field-free switching is observed only for a t_{Ti} up to 4 nm. Since the SOP spin current is found to retain the same sign, it can be concluded that it is primarily governed by the charge current flowing near the interface interacting with the spin–orbit field $\mathbf{B}_{so}$. Our results indicate that the field-free SOT switching current in magnetic trilayer structures can be further reduced by constructively combining the SOF and SOP spin currents through conductivity engineering.

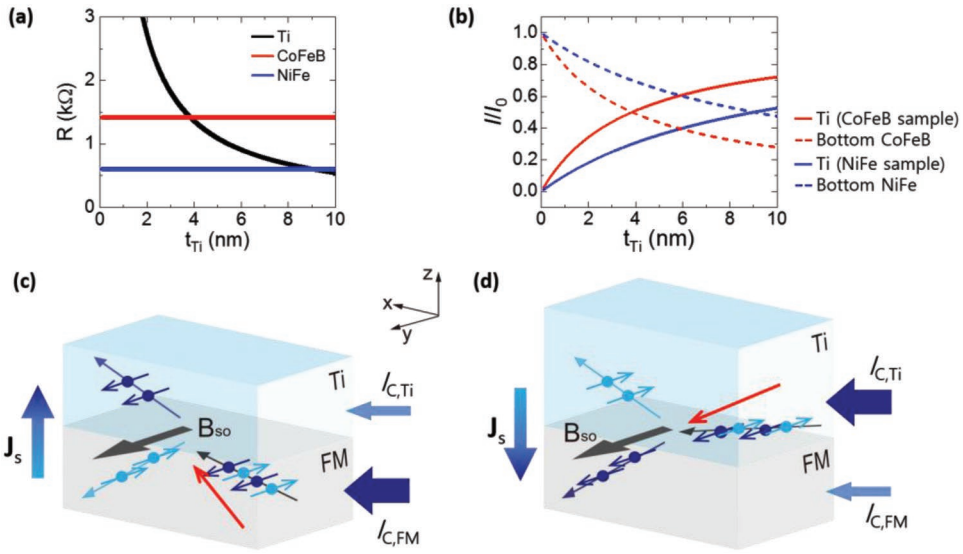

Figure 5. a) The resistance R of Ti (black line), CoFeB (red line), and NiFe (blue line) in the as a function of t_{Ti}. b) Relative charge current flowing through the Ti (FM) layer $I_{Ti(FM)}/I_0$ in the CoFeB-sample (red lines) and NiFe-sample (blue lines). Here, I_0 is the total current and $I_{Ti(FM)}$ is the current flowing to Ti (FM) layer. c,d) Illustration of the SOF spin currents in the Ti/FM structure with c) a thin Ti ($I_{c,\,Ti} < I_{c,\,FM}$)and d) a thick Ti ($I_{c,\,Ti} > I_{c,\,FM}$). When $I_{c,\,Ti} < I_{c,\,FM}$ ($I_{c,\,Ti} > I_{c,\,FM}$), the J_S is predominantly governed by the spin transmission (reflection) at the FM/Ti interface, with a spin polarization parallel (antiparallel) to the $\mathbf{B}_{so}$.

4. Experimental Section

Sample Preparation: Trilayer samples of FM (4 nm)/Ti (1–6 nm)/CoFeB (1 nm)/MgO (3.2 nm)/Ta (2 nm) structures were deposited on thermally oxidized Si substrates by magnetron sputtering with a base pressure below 3.0×10^{-8} Torr. To introduce the in-plane magnetic anisotropy of the bottom FM, an in-plane magnetic field of 15 mT was applied in the *x*-direction during deposition. The samples were post-annealed at 150 °C for 40 min to induce perpendicular magnetic anisotropy in the top CoFeB layer. Hall bar devices with a width of 5 µm and a length of 15 µm were fabricated using photolithography and Ar-ion milling. For the magnetization switching measurement, an FM island of 4 µm was defined within the Hall cross.

Electrical Measurement: A current pulse of 15 µs was applied in the current-induced magnetization switching experiment, and the anomalous Hall resistance was then measured at a dc current of 100 µA. The harmonic Hall voltage measurements were performed using lock-in amplifiers using an ac current I_{ac} with a frequency of 19.29 Hz to estimate the effective magnetic field induced by SOTs. The first and second harmonic Hall resistance were simultaneously measured while sweeping in-plane external magnetic fields in *x*-directions to the current direction. Note that the B_x was tilted slightly out of plane (≈2°) to prevent the formation of multidomains, and that thermal contributions were properly subtracted.

Supporting Information

Supporting Information is available from the Wiley Online Library or from the author.

Acknowledgements

This work was supported from Samsung Electronics Co., Ltd. (Grant No. IO200721-07533-01) (Development of interfacial SOT materials) and National Research Foundation of Korea (Grant Nos. NRF-2020R1A2C2010309 and 2022M3I7A2079267).

Conflict of Interest

The authors declare no conflict of interest.

Data Availability Statement

The data that support the findings of this study are available from the corresponding author upon reasonable request.

Keywords

field-free switching, interface-generated spin currents, MRAM, spin–orbit torque, spintronic applications

Received: June 14, 2022
Revised: September 22, 2022
Published online: November 13, 2022

[1] S. A. Wolf, D. D. Awschalom, R. A. Buhrman, J. M. Daughton, S. Von Molnár, M. L. Roukes, A. Y. Chtchelkanova, D. M. Treger, *Science* **2001**, *294*, 1488.
[2] I. Žutić, J. Fabian, S. D. Sarma, *Rev. Mod. Phys.* **2004**, *76*, 323.
[3] Q. Shao, P. Li, L. Liu, H. Yang, S. Fukami, A. Razavi, H. Wu, K. Wang, F. Freimuth, Y. Mokrousov, M. D. Stiles, S. Emori, A. Hoffmann, J. Akerman, K. Roy, J. P. Wang, S. H. Yang, K. Garello, W. Zhang, *IEEE Trans. Magn.* **2021**, *57*, 9427163.
[4] C. Chappert, A. Fert, F. N. Van Dau, *Nat. Mater.* **2007**, *6*, 813.
[5] A. Brataas, A. D. Kent, H. Ohno, *Nat. Mater.* **2012**, *11*, 372.
[6] S. Bhatti, R. Sbiaa, A. Hirohata, H. Ohno, S. Fukami, S. N. Piramanayagam, *Mater. Today* **2017**, *20*, 530.
[7] X. Qiu, Z. Shi, W. Fan, S. Zhou, H. Yang, *Adv. Mater.* **2018**, *30*, 1705699.

[8] R. Ramaswamy, J. M. Lee, K. Cai, H. Yang, *Appl. Phys. Rev.* **2018**, *5*, 031107.
[9] A. Manchon, J. Železný, I. M. Miron, T. Jungwirth, J. Sinova, A. Thiaville, K. Garello, P. Gambardella, *Rev. Mod. Phys.* **2019**, *91*, 035004.
[10] Y. Li, K. W. Edmonds, X. Liu, H. Zheng, K. Wang, *Adv. Quantum Technol.* **2019**, *2*, 1800052.
[11] J. Ryu, S. Lee, K.-J. Lee, B.-G. Park, *Adv. Mater.* **2020**, *32*, 1907148.
[12] J. Wunderlich, B. Kaestner, J. Sinova, T. Jungwirth, *Phys. Rev. Lett.* **2005**, *94*, 047204.
[13] A. Chernyshov, M. Overby, X. Liu, J. K. Furdyna, Y. Lyanda-Geller, L. P. Rokhinson, *Nat. Phys.* **2009**, *5*, 656.
[14] I. M. Miron, K. Garello, G. Gaudin, P.-J. Zermatten, M. V. Costache, S. Auffret, S. Bandiera, B. Rodmacq, A. Schuhl, P. Gambardella, *Nature* **2011**, *476*, 189.
[15] L. Liu, C. F. Pai, Y. Li, H. W. Tseng, D. C. Ralph, R. A. Buhrman, *Science* **2012**, *336*, 555.
[16] C. F. Pai, L. Liu, Y. Li, H. W. Tseng, D. C. Ralph, R. A. Buhrman, *Appl. Phys. Lett.* **2012**, *101*, 122404.
[17] J. Kim, J. Sinha, M. Hayashi, M. Yamanouchi, S. Fukami, T. Suzuki, S. Mitani, H. Ohno, *Nat. Mater.* **2013**, *12*, 240.
[18] A. Hoffmann, *IEEE Trans. Magn.* **2013**, *49*, 5172.
[19] M. M. Decker, M. S. Wörnle, A. Meisinger, M. Vogel, H. S. Körner, G. Y. Shi, C. Song, M. Kronseder, C. H. Back, *Phys. Rev. Lett.* **2017**, *118*, 257201.
[20] X. Shu, J. Zhou, J. Deng, W. Lin, J. Yu, L. Liu, C. Zhou, P. Yang, J. Chen, *Phys. Rev. Mater.* **2019**, *3*, 114410.
[21] H. Bai, X. F. Zhou, H. W. Zhang, W. W. Kong, L. Y. Liao, X. Y. Feng, X. Z. Chen, Y. F. You, Y. J. Zhou, L. Han, W. X. Zhu, F. Pan, X. L. Fan, C. Song, *Phys. Rev. B* **2021**, *104*, 104401.
[22] M. I. Dyakonov, V. I. Perel, *Phys. Lett. A* **1971**, *35*, 459.
[23] Y. A. Bychkov, E. I. Rashba, *J. Phys. C: Solid State Phys.* **1984**, *17*, 6039.
[24] V. M. Edelstein, *Solid State Commun.* **1990**, *73*, 233.
[25] S. D. Ganichev, V. V. Bel'kov, P. Schneider, S. Giglberger, S. N. Danilov, W. Weber, M. Olteanu, W. Prettl, *Semicond. Sci. Technol* **2008**, *23*, 114003.
[26] A. Manchon, S. Zhang, *Phys. Rev. B* **2008**, *78*, 212405.
[27] I. M. Miron, T. Moore, H. Szambolics, L. D. Buda-Prejbeanu, S. Auffret, B. Rodmacq, S. Pizzini, J. Vogel, M. Bonfim, A. Schuhl, G. Gaudin, *Nat. Mater.* **2011**, *10*, 419.
[28] I. M. Miron, G. Gaudin, S. Auffret, B. Rodmacq, A. Schuhl, S. Pizzini, J. Vogel, P. Gambardella, *Nat. Mater.* **2012**, *9*, 230.
[29] A. Manchon, H. C. Koo, J. Nitta, S. M. Frolov, R. A. Duine, *Nat. Mater.* **2015**, *14*, 871.
[30] G. Choi, J. Ryu, R. Thompson, J. G. Choi, J. Jeong, S. Lee, M. G. Kang, M. Kohda, J. Nitta, B. G. Park, *APL Mater.* **2022**, *10*, 011105.
[31] S. C. Baek, V. P. Amin, Y. W. Oh, G. Go, S.-J. Lee, G.-H. Lee, K.-J. Kim, M. D. Stiles, B.-G. Park, K.-J. Lee, *Nat. Mater.* **2018**, *17*, 509.
[32] V. P. Amin, J. Zemen, M. D. Stiles, *Phys. Rev. Lett.* **2018**, *121*, 136805.
[33] A. M. Humphries, T. Wang, E. R. J. Edwards, S. R. Allen, J. M. Shaw, H. T. Nembach, J. Q. Xiao, T. J. Silva, X. Fan, *Nat. Commun.* **2017**, *8*, 911.
[34] Y.-W. Oh, J. Ryu, J. Kang, B.-G. Park, *Adv. Electron. Mater.* **2019**, *5*, 1900598.
[35] J. Ryu, R. Thompson, J. Y. Park, S.-J. Kim, G. Choi, J. Kang, H. B. Jeong, M. Kohda, J. M. Yuk, J. Nitta, K.-J. Lee, B.-G. Park, *Nat. Electron.* **2022**, *5*, 217.
[36] Y. Sheng, K. W. Edmonds, X. Ma, H. Zheng, K. Wang, *Adv. Electron. Mater.* **2018**, *4*, 1800224.
[37] C. Sun, J. Deng, S. M. Rafi-Ul-Islam, G. Liang, H. Yang, M. B. A. Jalil, *Phys. Rev. Appl.* **2019**, *12*, 034022.
[38] Y. Li, J. Liang, H. Yang, H. Zheng, K. Wang, *Appl. Phys. Lett.* **2020**, *117*, 092404.
[39] Y. Hibino, K. Hasegawa, T. Koyama, D. Chiba, *APL Mater.* **2020**, *8*, 041110.
[40] Y. Hibino, T. Taniguchi, K. Yakushiji, A. Fukushima, H. Kubota, S. Yuasa, *Nat. Commun.* **2021**, *12*, 6254.
[41] W. Wang, Q. Fu, K. Zhou, L. Chen, L. Yang, Z. Li, Z. Tao, C. Yan, L. Liang, X. Zhan, Y. Du, R. Liu, *Phys. Rev. Appl.* **2022**, *17*, 034026.
[42] Y. Cao, A. W. Rushforth, Y. Sheng, H. Zheng, K. Wang, *Adv. Funct. Mater.* **2019**, *29*, 1808104.
[43] Q. Ma, Y. Li, D. B. Gopman, Y. P. Kabanov, R. D. Shull, C. L. Chien, *Phys. Rev. Lett.* **2018**, *120*, 117703.
[44] Y. C. Lau, D. Betto, K. Rode, J. M. D. Coey, P. Stamenov, *Nat. Nanotechnol.* **2016**, *11*, 758.
[45] L. Liu, C. Zhou, X. Shu, C. Li, T. Zhao, W. Lin, J. Deng, Q. Xie, S. Chen, J. Zhou, R. Guo, H. Wang, J. Yu, S. Shi, P. Yang, S. Pennycook, A. Manchon, J. Chen, *Nat. Nanotechnol.* **2021**, *16*, 277.
[46] K. Cai, M. Yang, H. Ju, S. Wang, Y. Ji, B. Li, K. W. Edmonds, Y. Sheng, B. Zhang, N. Zhang, S. Liu, H. Zheng, K. Wang, *Nat. Mater.* **2017**, *16*, 712.
[47] L. You, O. J. Lee, D. Bhowmik, D. Labanowski, J. Hong, J. Bokor, S. Salahuddin, *Proc. Natl. Acad. Sci. USA* **2015**, *112*, 10310.
[48] W. J. Kong, C. H. Wan, X. Wang, B. S. Tao, L. Huang, C. Fang, C. Y. Guo, Y. Guang, M. Irfan, X. F. Han, *Nat. Commun.* **2019**, *10*, 233.
[49] Y. Cao, Y. Sheng, K. W. Edmonds, Y. Ji, H. Zheng, K. Wang, *Adv. Mater.* **2020**, *32*, 1907929.
[50] G. Yu, P. Upadhyaya, Y. Fan, J. G. Alzate, W. Jiang, K. L. Wong, S. Takei, S. A. Bender, L. Chang, Y. Jiang, M. Lang, J. Tang, Y. Wang, Y. Tserkovnyak, P. K. Amiri, K. L. Wang, *Nat. Nanotechnol.* **2014**, *9*, 548.
[51] Z. A. Bekele, X. Liu, Y. Cao, K. Wang, *Adv. Electron. Mater.* **2021**, *7*, 2000793.
[52] X. Shu, L. Liu, J. Zhou, W. Lin, Q. Xie, T. Zhao, C. Zhou, S. Chen, H. Wang, J. Chai, Y. Ding, W. Chen, J. Chen, *Phys. Rev. Appl.* **2022**, *17*, 024031.
[53] K. Garello, C. O. Avci, I. M. Miron, M. Baumgartner, A. Ghosh, S. Auffret, O. Boulle, G. Gaudin, P. Gambardella, *Appl. Phys. Lett.* **2014**, *105*, 212402.
[54] Y.-W. Oh, S. C. Baek, Y. M. Kim, H.-Y. Lee, K.-D. Lee, C.-G. Yang, E.-S. Park, K.-S. Lee, K.-W. Kim, G. Go, J.-R. Jeong, B.-C. Min, H.-W. Lee, K.-J. Lee, B.-G. Park, *Nat. Nanotechnol.* **2016**, *11*, 878.
[55] S. Fukami, C. Zhang, S. Duttagupta, A. Kurenkov, H. Ohno, *Nat. Mater.* **2016**, *15*, 535.
[56] M. Baumgartner, K. Garello, J. Mendil, C. O. Avci, E. Grimaldi, C. Murer, J. Feng, M. Gabureac, C. Stamm, Y. Acremann, S. Finizio, S. Wintz, J. Raabe, P. Gambardella, *Nat. Nanotechnol.* **2017**, *12*, 980.
[57] G. Y. Shi, C. H. Wan, Y. S. Chang, F. Li, X. J. Zhou, P. X. Zhang, J. W. Cai, X. F. Han, F. Pan, C. Song, *Phys. Rev. B* **2017**, *95*, 104435.
[58] L. Ren, L. Liu, X. Shu, W. Lin, P. Yang, J. Chen, K. L. Teo, *ACS Appl. Mater. Interfaces* **2021**, *13*, 18294.
[59] B. F. Miao, S. Y. Huang, D. Qu, C. L. Chien, *Phys. Rev. Lett.* **2013**, *111*, 066602.
[60] A. Tsukahara, Y. Ando, Y. Kitamura, H. Emoto, E. Shikoh, M. P. Delmo, T. Shinjo, M. Shiraishi, *Phys. Rev. B* **2014**, *89*, 235317.
[61] G. Qu, K. Nakamura, M. Hayashi, *Phys. Rev. B* **2020**, *102*, 144440.
[62] A. Mook, R. R. Neumann, A. Johansson, J. Henk, I. Mertig, *Phys. Rev. Res.* **2020**, *2*, 023065.
[63] L. Salemi, P. M. Oppeneer, *Phys. Rev. B* **2022**, *106*, 024410.
[64] M. Kimata, H. Chen, K. Kondou, S. Sugimoto, P. K. Muduli, M. Ikhlas, Y. Omori, T. Tomita, A. H. MacDonald, S. Nakatsuji, Y. Otani, *Nature* **2019**, *565*, 627.
[65] M. B. Lifshits, M. I. Dyakonov, *Phys. Rev. Lett.* **2009**, *103*, 186601.

[66] C. O. Pauyac, M. Chshiev, A. Manchon, S. A. Nikolaev, *Phys. Rev. Lett.* **2018**, *120*, 176802.
[67] U. H. Pi, K. W. Kim, J. Y. Bae, S. C. Lee, Y. J. Cho, K. S. Kim, S. Seo, *Appl. Phys. Lett.* **2010**, *97*, 162507.
[68] K. Garello, I. M. Miron, C. O. Avci, F. Freimuth, Y. Mokrousov, S. Blügel, S. Auffret, O. Boulle, G. Gaudin, P. Gambardella, *Nat. Nanotechnol.* **2013**, *8*, 587.
[69] M. Hayashi, J. Kim, M. Yamanouchi, H. Ohno, *Phys. Rev. B* **2014**, *89*, 144425.
[70] S. Woo, M. Mann, A. J. Tan, L. Caretta, G. S. D. Beach, *Appl. Phys. Lett.* **2016**, *105*, 212404.
[71] J. Kim, P. Sheng, S. Takahashi, S. Mitani, M. Hayashi, *Phys. Rev. Lett.* **2016**, *116*, 097201.
[72] M. H. Nguyen, C. F. Pai, K. X. Nguyen, D. A. Muller, D. C. Ralph, R. A. Buhrman, *Appl. Phys. Lett.* **2015**, *106*, 222402.
[73] M. Nguyen, D. C. Ralph, R. A. Buhrman, *Phys. Rev. Lett.* **2016**, *116*, 126601.
[74] J. Ryu, M. Kohda, J. Nitta, *Phys. Rev. Lett.* **2016**, *116*, 256802.